J|A|C|S
COMMUNICATIONS

Published on Web 10/14/2006

A Low-Spin Alkylperoxo−Iron(III) Complex with Weak Fe−O and O−O Bonds: Implications for the Mechanism of Superoxide Reductase

Divya Krishnamurthy,† Gary D. Kasper,† Frances Namuswe,† William D. Kerber,† Amy A. Narducci Sarjeant,† Pierre Moënne-Loccoz,*,‡ and David P. Goldberg*,†

Department of Chemistry, Johns Hopkins University, Baltimore, Maryland 21218, and Department of Environmental and Biomolecular Systems, OGI School of Science and Engineering, Oregon Health & Science University, Beaverton, Oregon, 97006

Received June 26, 2006; E-mail: dpg@jhu.edu; ploccoz@ebs.ogi.edu

Until recently, the removal of superoxide anion (O_2^-) from the biological milieu was believed to take place almost exclusively through the action of the superoxide dismutases. The discovery of superoxide reductase[1] (SOR), a mononuclear iron enzyme that converts O_2^- to H_2O_2 via a one-electron reduction pathway, has altered this view. The active site of SOR is unique, being comprised of a [$(N_{His})_4(S_{cys})Fe^{II}$] center (reduced active form, SOR_{red}). The four neutral N donors are positioned in the equatorial plane of a square pyramid, while the thiolate donor occupies an axial position trans to the putative O_2^- binding site. Thus, the iron coordination sphere in SOR resembles that of the heme iron in cytochrome P450. Spectroscopic evidence suggests that an Fe^{III}−OO(H) intermediate forms during SOR turnover,[1] but unlike in P450, where this species undergoes O−O bond cleavage to form a high-valent Fe=O species, the hydroperoxo group is released as H_2O_2 after protonation. It has been suggested that the spin state of the Fe^{III}−OO(H) intermediate ($S = {}^1/_2$ vs ${}^5/_2$) may play an important role in determining the outcome of this reaction,[1b,2] but the mechanism of action of SOR and, in particular, the factors that account for the dramatically different outcomes of the chemistry of SOR versus P450 remain to be determined.

A few model complexes of SOR have recently emerged, including an example of an Fe^{III}−OOH species ($S = {}^1/_2$) that contains thiolate ligation[3] and a high-spin [$N_4S_{thiolate}$]Fe^{III}−OO*t*Bu complex.[2d] Here, we report the synthesis of a novel analogue of SOR_{red}, [([15]aneN_4)Fe^{II}(SPh)]BF_4 (**1**), and its reactivity with alkylperoxides. Specifically, we have characterized a low-spin [$N_4S_{thiolate}$]Fe^{III}−OOR intermediate which exhibits a bonding pattern that is dramatically different from those of all previously characterized low-spin Fe^{III}−OOR species.

The iron(II) complex **1** is obtained by reaction of [15]aneN_4 with $Fe^{II}(BF_4)_2$ followed by addition of NaSPh (Scheme 1). The structure of **1** (Figure 1) reveals that a single phenylthiolate ligand is coordinated to the iron(II) center, resulting in a five-coordinate geometry between that of square pyramidal (sp) and trigonal bipyramidal (tbp) ($\tau = 0.49$).[4] The four neutral nitrogen donors and one thiolate ligand match the donor set found in SOR_{red}, although the geometry is closer to sp in the enzyme. A similar self-assembly reaction was used to prepare the SOR_{red} model [(Me_4-cyclam)Fe^{II}(SPh-*p*-OMe)]$^+$, which also exhibits a distorted geometry between sp and tbp ($\tau = 0.50$).[5a] The Fe−N and Fe−S bond lengths for **1** are in line with other Fe^{II}−N and Fe^{II}−S bond distances for high-spin iron(II).[6] The N−H groups are arranged so that H(2) points toward the axial thiolate ligand, while H(1), H(3), and H(4) lie on the opposite side of the macrocyclic plane. The NH(2)−S(1′) and N(2)−S(1′) distances of 2.60(5) and 3.489(4) Å,

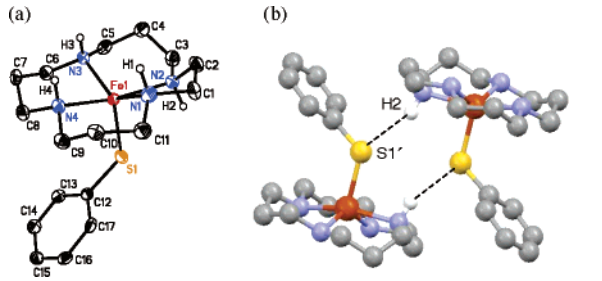

Figure 1. (a) ORTEP diagram of the cation of **1** showing 50% probability ellipsoids with some of the hydrogen atoms omitted for clarity. Selected bond lengths (Å): Fe(1)−N(1) 2.164(3), Fe(1)−N(2) 2.273(3), Fe(1)−N(3) 2.138(3), Fe(1)−N(4) 2.206(3), Fe(1)−S(1) 2.3316(11). (b) Packing diagram highlighting the intermolecular NH−S hydrogen bonds.

Scheme 1

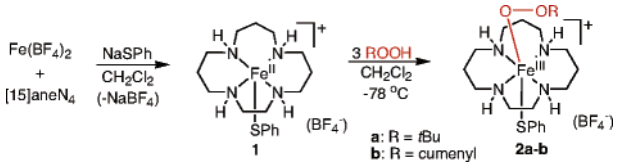

together with an N(2)−H(2)−S(1′) angle of 158(3)°, provide good evidence for the presence of an intermolecular N−H−S hydrogen bond. It is not known at this time if these intermolecular H-bonds persist in solution, but it is worth noting that, in SOR, the coordinating S_{Cys} appears to be hydrogen bonded to two N−$H_{peptide}$ groups.[1a]

Reaction of **1** with the alkyl hydroperoxides *t*BuOOH or cumeneOOH in CH_2Cl_2 at low temperature (−78 °C) leads to the formation of dark red intermediates **2a** (*t*BuOOH) and **2b** (cumenylOOH) (Scheme 1). These dark red species, not observed at room temperature, exhibit relatively short lifetimes at −80 °C (**2a**: $k_{obs} = 5.4 \times 10^{-3}$ s^{-1}), persisting for ∼10 min at −80 °C. This brief window of stability was enough to characterize the red intermediate by low-temperature UV−vis spectroscopy. The red intermediate for the *t*BuOOH reaction gives rise to a 526 nm absorbance ($\epsilon = 2150$ M^{-1} cm^{-1} assuming total conversion of **1** to **2a**) (Figure 2). In comparison, the cumenyl derivative exhibits a λ_{max} at 527 nm ($\epsilon = 1650$ M^{-1} cm^{-1}). Both the position and intensity of these bands are indicative of alkylperoxo-to-iron(III) LMCT transitions, suggesting that the red intermediate is an Fe^{III}−OOR complex.[2d,7]

The EPR spectra of **2a**,**b** reveal characteristic patterns of low-spin iron(III) complexes, with $g = 2.20$ and 1.97 (Figure S1).[8] Definitive identification of the chromophoric intermediate as an Fe^{III}−OOR species is provided by resonance Raman (RR) spectra obtained with a 514 nm excitation in the transient absorption. The RR spectrum of **2a** exhibits bands at 439, 483, 612, and 803 cm^{-1}

† Johns Hopkins University.
‡ Oregon Health & Science University.

10.1021/ja064525o CCC: $33.50

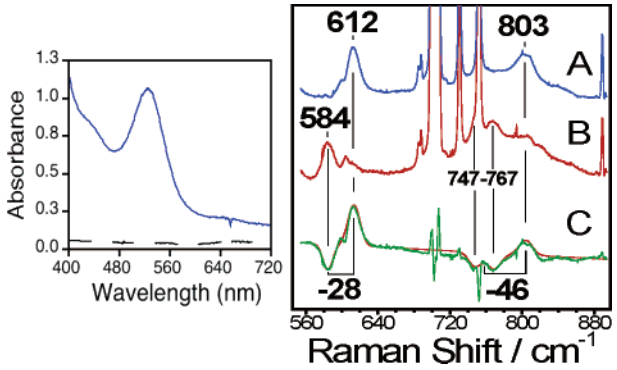

Figure 2. UV−vis spectra of **1** (black, dashed line) and **2a** (blue, solid line) in CH_2Cl_2 at −80 °C, and RR spectra of ^{16}O−**2a** (A) and ^{18}O−**2a** (B). The ^{16}O−^{18}O difference spectrum (C, green) is overlapped with a simulated trace composed of Gaussian peaks (C, red).

Table 1. Spin States and Vibrational Data for Fe^{III}−OOR Species

complex	spin state[a]	ν_{Fe-O} (cm^{-1})	ν_{O-O} (cm^{-1})	ref
$[Fe^{III}([15]aneN_4)(SPh)(OOtBu)]^+$	LS	612	803	*b*
$[Fe^{III}([15]aneN_4)(SPh)(OOCm)]^+$	LS	615	795	*b*
$[Fe^{III}(TPA)(OH_x)(OOtBu)]^{x+}$	LS	696	796	7f
$[Fe^{III}(L^8py_2)(SAr)(OOtBu)]^+$	HS	623	830, 874	2d

[a] LS = low-spin ($S = {}^1/_2$); HS = high-spin ($S = {}^5/_2$). [b] This work.

(Figures 2A and S2-A). Intermediate **2b** displays similar frequencies at 430, 490, 615, and 795 cm^{-1} (Figure S2-B). On the basis of earlier studies,[7] signals below 500 cm^{-1} can be assigned to (C−C−C) and (C−C−O) deformation modes of the alkylperoxo ligand. The bands at 803 and 795 cm^{-1} are within the expected range of O−O stretching vibrations in metal−alkylperoxo complexes, and they compare well with other low-spin Fe^{III}−OOR species (Table 1). In contrast, O−O stretching modes from high-spin Fe^{III}−OOR species are higher in energy, as seen in Table 1. RR bands at 612 cm^{-1} for **2a** and 615 cm^{-1} for **2b** are consistent with Fe−O stretching vibrations, but they are *dramatically lower in energy* than those observed for low-spin Fe^{III}−OOR adducts.[2d,7]

To confirm these assignments, intermediate **2a** was prepared with $tBu^{18}O^{18}OH$. The RR spectrum of ^{18}O-labeled **2a** is shown in Figure 2B (middle), along with the ^{18}O−^{16}O difference spectrum. The ν(Fe−^{18}O) is observed at 584 cm^{-1} which represents a 28 cm^{-1} ^{18}O-downshift. The $\nu(^{18}O-^{18}O)$ is downshifted 46 cm^{-1} and splits as a Fermi doublet centered at 757 cm^{-1} (Figure 2B). These ^{18}O-shifts are in complete agreement with those expected for isolated Fe−O and O−O diatomic oscillators. In contrast, vibrations observed below 500 cm^{-1} show only marginal ^{18}O-shifts, consistent with their assignment to alkyl C−C−C and C−C−O deformation modes (Figure S3). The perfect match between observed ^{18}O-shifts and predicted values for isolated diatomics supports an analysis of the observed ν(Fe−O) and ν(O−O) frequencies as group vibrations and permits correlations between vibrational frequencies and bond strengths.

Many mononuclear non-heme iron enzymes have been proposed to proceed via Fe^{III}−OOH reaction intermediates. Experimental and theoretical work on enzymes and models have led to a widely invoked hypothesis regarding spin state and Fe−O and O−O bond strengths in Fe^{III}−OOR complexes.[2d,7] Low-spin intermediates have been shown to exhibit high ν(Fe−O) and low ν(O−O), suggesting *strong* Fe−O and *weak* O−O bonds, respectively, while high-spin species exhibit the opposite pattern (Table 1). This trend is in agreement with the presumed mechanism of cytochrome P450 in which a low-spin Fe^{III}−OO(H) leads to O−O cleavage and formation of a high-valent Fe=O intermediate. In SOR, a high-spin Fe^{3+}−OO(H) intermediate with a weak Fe−O bond could favor H_2O_2 release rather than O−O bond cleavage.[2]

The vibrational signatures of intermediates **2a** and **2b** show that these Fe^{III}−OOR species exhibit *weak Fe−O bonds*, in sharp contrast with the data from other low-spin Fe^{III}−OOR complexes. The weaker Fe−O bonds in **2** may be due to a trans effect from the sulfur ligand, provided it is coordinated trans and not cis to the peroxide.[9] The sulfur ligand is believed to remain coordinated to the iron in **2** since preliminary experiments with substituted arylthiolate ligands show shifted transient absorption maxima (data not shown). Interestingly, recent DFT calculations have determined that a low-spin Fe^{III}−OOH intermediate should be energetically favored for SOR.[2a] Our results support these predictions and the possibility of a low-spin intermediate with a weak Fe−O bond in the course of O_2^- reduction by SOR.

Acknowledgment. We thank the NIH for financial support (D.P.G., GM62309; P.M.L., GM074785). W.D.K. is grateful for a Dreyfus Environmental Postdoctoral Fellowship. We thank K. D. Karlin for the use of his low-temperature UV−vis instrumentation.

Supporting Information Available: Experimental details, EPR spectra, RR data, and X-ray structure files for **1** (CIF). This material is available free of charge via the Internet at http://pubs.acs.org.

References

(1) (a) Kurtz, D. M., Jr. *Acc. Chem. Res.* **2004**, *37*, 902−908. (b) Mathé, C.; Nivière, V.; Houée-Levin, C.; Mattioli, T. A. *Biophys. Chem.* **2006**, *119*, 38−48. (c) Clay, M. D.; Yang, T. C.; Jenney, F. E., Jr.; Kung, I. Y.; Cosper, C. A.; Krishnan, R.; Kurtz, D. M., Jr.; Adams, M. W. W.; Hoffman, B. M.; Johnson, M. K. *Biochemistry* **2006**, *45*, 427−438. (d) Yeh, A. P.; Hu, Y.; Jenney, F. E., Jr.; Adams, M. W. W.; Rees, D. C. *Biochemistry* **2000**, *39*, 2499−2508.

(2) (a) Silaghi-Dumitrescu, R.; Silaghi-Dumitrescu, I.; Coulter, E. D.; Kurtz, D. M., Jr. *Inorg. Chem.* **2003**, *42*, 446−456. (b) Clay, M. D.; Cosper, C. A.; Jenney, F. E., Jr.; Adams, M. W. W.; Johnson, M. K. *Proc. Natl. Acad. Sci. U.S.A.* **2003**, *100*, 3796−3801. (c) Kovacs, J. A. *Chem. Rev.* **2004**, *104*, 825−848. (d) Bukowski, M. R.; Halfen, H. L.; van den Berg, T. A.; Halfen, J. A.; Que, L., Jr. *Angew. Chem., Int. Ed.* **2005**, *44*, 584−587.

(3) Theisen, R. M.; Kovacs, J. A. *Inorg. Chem.* **2005**, *44*, 1169−1171.

(4) Addison, A. W.; Rao, T. N.; Reedjik, J.; van Rijn, J.; Verschoor, G. C. *J. Chem. Soc., Dalton Trans.* **1984**, 1349−1456.

(5) (a) Fiedler, A. T.; Halfen, H. L.; Halfen, J. A.; Brunold, T. C. *J. Am. Chem. Soc.* **2005**, *127*, 1675−1689. (b) For examples of related zinc(II) complexes, see: Notni, J.; Gorls, H.; Anders, E. *Eur. J. Inorg. Chem.* **2006**, 1444−1455.

(6) Krishnamurthy, D.; Sarjeant, A.; Goldberg, D. P.; Caneschi, A.; Totti, F.; Zakharov, L. N.; Rheingold, A. L. *Chem.—Eur. J.* **2005**, *11*, 7328−7341 and references therein.

(7) (a) Menage, S.; Wilkinson, E. C.; Que, L., Jr.; Fontecave, M. *Angew. Chem., Int. Ed.* **1995**, *34*, 203−205. (b) Zang, Y.; Kim, J.; Dong, Y. H.; Wilkinson, E. C.; Appelman, E. H.; Que, L., Jr. *J. Am. Chem. Soc.* **1997**, *119*, 4197−4205. (c) Wada, A.; Ogo, S.; Watanabe, Y.; Mukai, M.; Kitagawa, T.; Jitsukawa, K.; Masuda, H.; Einaga, H. *Inorg. Chem.* **1999**, *38*, 3592−3593. (d) Girerd, J. J.; Banse, F.; Simaan, A. *J. Struct. Bonding* **2000**, *97*, 145−177. (e) Lehnert, N.; Ho, R. Y. N.; Que, L., Jr.; Solomon, E. I. *J. Am. Chem. Soc.* **2001**, *123*, 12802−12816. (f) Lehnert, N.; Ho, R. Y. N.; Que, L., Jr.; Solomon, E. I. *J. Am. Chem. Soc.* **2001**, *123*, 8271−8290. (g) Lehnert, N.; Fujisawa, K.; Solomon, E. I. *Inorg. Chem.* **2003**, *42*, 469−481.

(8) Quantitation of the low-spin EPR signal reveals that it accounts for 10−30% of the starting iron(II) complex. This relatively low value is likely due to decay of the Fe^{III}−OOR species during the manual mixing time in the EPR tube. In contrast, the UV−vis spectra for **2** are obtained within a few seconds after addition of ROOH. Moreover, the ~5-fold increase in concentration of reactants in the EPR experiments compared to those used in the UV−vis will accelerate intermolecular decay pathways. Thus, it is reasonable to estimate ϵ values for **2** based on 100% conversion despite the EPR quantitation measurements.

(9) Deuteration of **1** at the N−H positions does not change the ν(Fe−O), ruling out hydrogen bonding as the cause of the low frequency.

JA064525O